Available online at www.sciencedirect.com

jmr&t Journal of Materials Research and Technology

journal homepage: www.elsevier.com/locate/jmrt

Original Article

# Influence of eutectic phase precipitation on cracking susceptibility during forging of a martensitic stainless steel for turbine shaft applications

S. Dourandish [a,*], M. Jahazi [a,**], G.R. Ebrahimi [b], L. Ebacher [c]

[a] Department of Mechanical Engineering, École de Technologie Supériere, 1100 Notre-Dame West, Montreal, Quebec, H3C 1K3, Canada

[b] Materials and Metallurgical Engineering Department, Faculty of Engineering, Ferdowsi University of Mashhad, Mashhad, 9177948974, Iran

[c] Finkl Steel-Sorel Inc., 100 McCarthy, Saint-Joseph-de-Sorel, Québec, J3R 3M8, Canada

ARTICLE INFO

*Article history:*
Received 30 November 2020
Accepted 26 April 2021
Available online 1 May 2021

*Keywords:*
Martensitic stainless steel
Eutectic carbide
Solidification
Hot working
Electron backscatter diffraction (EBSD) analysis

ABSTRACT

The presence of the eutectic phase (delta ferrite + $M_{23}C_6$) in martensitic stainless steels brings significant deterioration of the in-service mechanical properties of the critical components such as turbine shaft made of these alloys. In the present study, thermodynamic and kinetics of eutectic phase formation during solidification and the reheating stages before forging of a large size X38CrMo16 martensitic stainless steel ingot are investigated. Material characterization and microstructural evolution were characterized in three different zones of a large size ingot. It was observed that the forging temperature and the solidification rate were the two most effective parameters influencing the volume fraction of the eutectic phase and its morphology. Optical and electron microscopy observations along with Energy Dispersion Spectroscopy (EDS) and Electron Backscatter Diffraction (EBSD) measurements were used in the investigation. The results showed that the eutectic phase precipitated primarily at the grain boundaries. Furthermore, a clear evolution on the morphology and volume fraction of the eutectic phase including thin film-like and skeleton-like carbides was found from the outer surface to the center of the ingot along the radial direction. EDS analysis revealed the substantial presence of chromium, molybdenum, and carbon within the $M_{23}C_6$ along the grain boundaries. Phase transformation and the precipitation phase sequences were analyzed as a function of temperature and composition of eutectic transformation using the Thermo-Calc software and the predictions were validated with experimental findings.



* Corresponding author.
** Corresponding author.
E-mail addresses: simin.dourandish.1@ens.etsmtl.ca (S. Dourandish), mohammad.Jahazi@etsmtl.ca (M. Jahazi).

https://doi.org/10.1016/j.jmrt.2021.04.075

## 1. Introduction

Martensitic Stainless Steels (MSS) belong to the family of high strength alloys and are widely used for rotors, turbine shafts, and pump bodies due to their good balance of high strength, ductility, and corrosion resistance [1]. The casting process of the large size ingots of a metallic alloy is an industrial challenge due to the occurrence of macrosegregation during solidification especially at the center of the ingot [2]. Besides, variable macrostructures including very fine grains in the chill zone, columnar grains, and equiaxed grains can be seen along the radial direction of the cast ingot [3]. These inhomogeneities of alloying elements distribution and macrostructure can modify thermophysical properties [4] and microstructure [5,6].

MSS are rarely used in the as-cast state and the cast ingots generally go through an open-die forging process carried out at temperatures about 0.75 of the melting point of the alloy. Finally, normalization, quenching and tempering treatments followed by machining operations are applied to obtain the final component (e.g. Turbine shafts). Prior to the open die forging operation, cast ingots are reheated for tens of hours, in the case of large size ingots, to reach the forging temperature. Therefore, the selection of the reheating/forging temperature is of critical importance to achieve the full breakdown of the as-cast dendritic structure, eliminate solidification porosities, and reduce the chemical (macrosegregation) inhomogeneity [7,8].

The post forge microstructure is generally composed of martensite, delta ferrite, and carbides [9]. Among these phases, delta ferrite is formed at high temperatures and its volume fraction, morphology and distribution could have a significant impact on the quality of the final product. For example, it has been reported that increasing the content of the delta ferrite deteriorates the impact properties, decreases tensile strength, ductility, and toughness [10–13]. In addition to delta ferrite, carbides formed during solidification of MSS and coarse carbides in the microstructure act as a preferential site for crack initiation and deteriorates the corrosion resistance of the alloy. Finally, the combined presence of delta ferrite and coarse carbides could significantly reduce the formability of the alloy during high temperature forming operations [14]. Specifically, Qi et al. reported that the size, morphology, volume fraction, and distribution of the eutectic phase are always a big challenge in heavy forging of MSS and are often associated with crack propagation during deformation, which may result in scrapping of large size components [15]. The present research work was initiated following observation of cracks after forging of a 21 metric tons X38CrMo 16 martensitic stainless steel ingot with the view to understand the fundamental relations between process parameters and microstructure evolution and prevent future cracking.

The eutectic phase precipitation is the result of the decomposition of liquid to two solid phases at the final solidifying phase [16]. Boccalini et al. investigated the effects of the chemical composition and cooling rate on the development of the solidified microstructure of high-speed steel. They reported that the solidification sequence started with the precipitation of primary delta ferrite from liquid followed by the formation of austenite through a peritectic reaction and then proceeded to the formation of eutectic carbides, $M_2C$, $M_6C$, and MC, through a eutectic reaction. It has also been reported that the total eutectic volume fraction increases with increasing the carbon content, W/Mo ratio, V content, and decreasing cooling rate [17]. Guo et al. investigated the precipitation sequence of different phases during the solidification of a high chromium steel ingot. The DSC curve and isopleth diagram revealed that the primary austenite formed in the liquid at 1380 °C, then the eutectic reaction occurred in the residual liquid with the eutectic phase composed of austenite + carbide and distributed along the grain boundary [18]. Zhou et al. studied the effect of cooling rate during solidification on the characteristics of the eutectic phase. They reported that at a low cooling rate, 0.9 K/s, eutectic carbides presented a needle-like or lamellar shape while with increasing cooling rates, the carbides developed into a rod-like shape [19]. It must be mentioned that the solidification sequence in MSS is off eutectic, which means that first delta ferrite phase forms from liquid followed by the formation of austenite then carbide [20]. Off-eutectic solidification starting with the initial formation of $\gamma$ dendrites, followed by a eutectic reaction of $L \rightarrow \gamma + MC$ has also been reported for other alloys, such as IN718 [21]. Some investigations have shown that the precipitation of eutectic carbides could only occur under slow cooling rates or during aging treatments and that fast cooling, suppresses its formation [22,23].

Despite the significant impact of the formation and characteristics of the eutectic phases during solidification of martensitic stainless steels, there is very little data available in the literature on macro and microstructural characterization of the above phases in the cast state of these steels. The present work addresses this aspect and investigates the influence of forging temperature on the characteristics of eutectic phases in a large casting made of X38CrMo16 martensitic stainless steel. More specifically, the investigation focuses on establishing possible correlations between the characteristics of the eutectic phases and the cracks observed during the forging of the ingot. For this purpose, advanced characterization techniques were used to determine the phase distribution, chemical composition, phase identification, and morphology in three different zones of the ingot. Moreover, a thermodynamic simulation was utilized to determine the formation region of each phase at the forging temperature and the corresponding eutectic composition. The experimental investigation results were then correlated with the thermodynamic simulation to

**Table 1 – Chemical composition of X38CrMo16 used in this investigation (wt. %).**

| Element | C | Mn | P | S | Si | Ni | Cr | Mo | Cu | Fe |
|---|---|---|---|---|---|---|---|---|---|---|
| Content | 0.37 | 0.88 | 0.03 | 0.024 | 0.32 | 0.48 | 15.21 | 1.1 | 0.042 | Bal. |

optimize the selection of the forging temperatures and minimize defect generation.

## 2. Method

The chemical composition of the samples, X38CrMo16 MSS, were determined using a SPECTROMAXx, Optical Emission Mass Spectrometer. Three measurements were made for each sample and the average value was used, Table 1. The microstructural characterization was carried out for two different forging temperatures, 1204 °C and 1260 °C. These temperatures were selected based on a preliminary study that allowed to narrow the 'optimum' temperature for the reheating stage of the castings before the open-die forging operation.

The samples were provided by Finkl Steel-Sorel, Quebec, Canada. The production cycle starts with melting using a 45-ton electric arc furnace followed by ladle metallurgy degassing and refining processes along with tight control of the chemical composition. The casting process is bottom pouring the molten steel at about 1570 °C into the mold. The solidified ingot is then taken to the forge furnace and heat up to the forging temperature (1200 °C–1260 °C). The next step after forging is heat treating of the sample through the quench and tempering cycle.

The samples used for the present investigation were cut from the center (C), quarter (Q), and surface (S) of the final round product forging at 1204 °C and from the center of the final round product forging at 1260 °C in the as-annealed condition, as shown in Fig. 1. Two different forging temperatures were used on two different ingots but with the same chemical composition, forge plan, and heat treatment. The heat treatment for both ingots started with holding the ingots at 537.77 °C for 65 h then followed by annealing at 954.44 °C for 17 h and cooling approximately 14.17 °C/h until 343.33 °C. Finally, tempering was done at 648.88 °C with 1.5hr/in.

The specimens were individually mounted and polished from 600 to 1200 grade SiC paper, then finished with 1 μm diamond grain paste. To reveal the microstructure, as-annealed samples were etched with Villela solution composed of 1 gr $(O_2N)_3C_6H_2OH$, 5 ml HCL, and 100 ml $C_2H_5OH$ for approximately 25 s. For microstructural characterizations, an Olympus LEXT OLS4100 laser confocal microscope was used. For scanning electron microscopy characterizations, a Hitachi SU8230, at 10 kV and 5 kV equipped with Brukers energy-dispersive spectroscopy EDS Quad detector (QUANTAX FlatQUAD) was employed. The phase identification of the microstructure was examined by a SU-8230 HITACHI equipped with a Bruker $e^-$Flash $HR^+$ electron backscatter diffraction (EBSD) detector using 10 kV and a pixel size of 64.9 nm. The total map size and working distance were 3158 $\mu m^2$ surface area and 15 mm respectively. The EBSD data were post-processed using QUANTAX ESPRIT software. For the EBSD analysis, the specimens were mechanically polished down to 0.5 μm. Then, the residual fine scratches and deformed surfaces were eliminated using an IM4000Plus ion milling system under 6 kV accelerating voltage and 25 rpm rotation speed for 40 min.

The XRD measurement was carried out using X'Pert3 MRD PANalytical with Cu Kα radiation (λ = 1.541 A°) with an angle between 20 and 90° (2-theta), the step size of 0.02° and use of monochromator. Also, Thermo-Calc thermodynamic software with steel and Fe-Alloy database and 2020a version was employed to simulate the phase diagrams and phase proportions over a wide range of temperatures and chemical compositions.

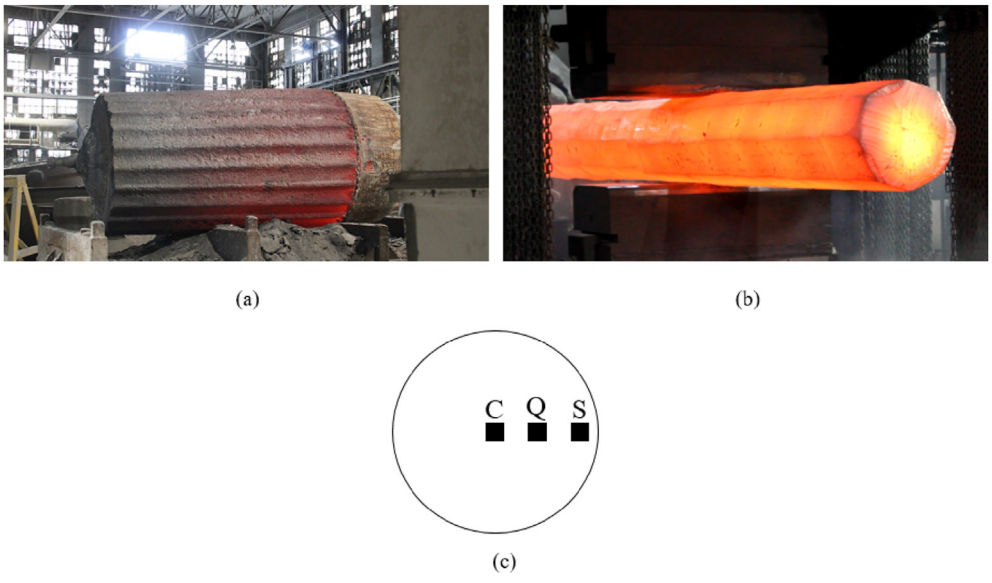


**Fig.1 – (a), As-cast ingot. (b), As-forged ingot. (c), Schematic illustration depicting the sample location used in material characterization.**

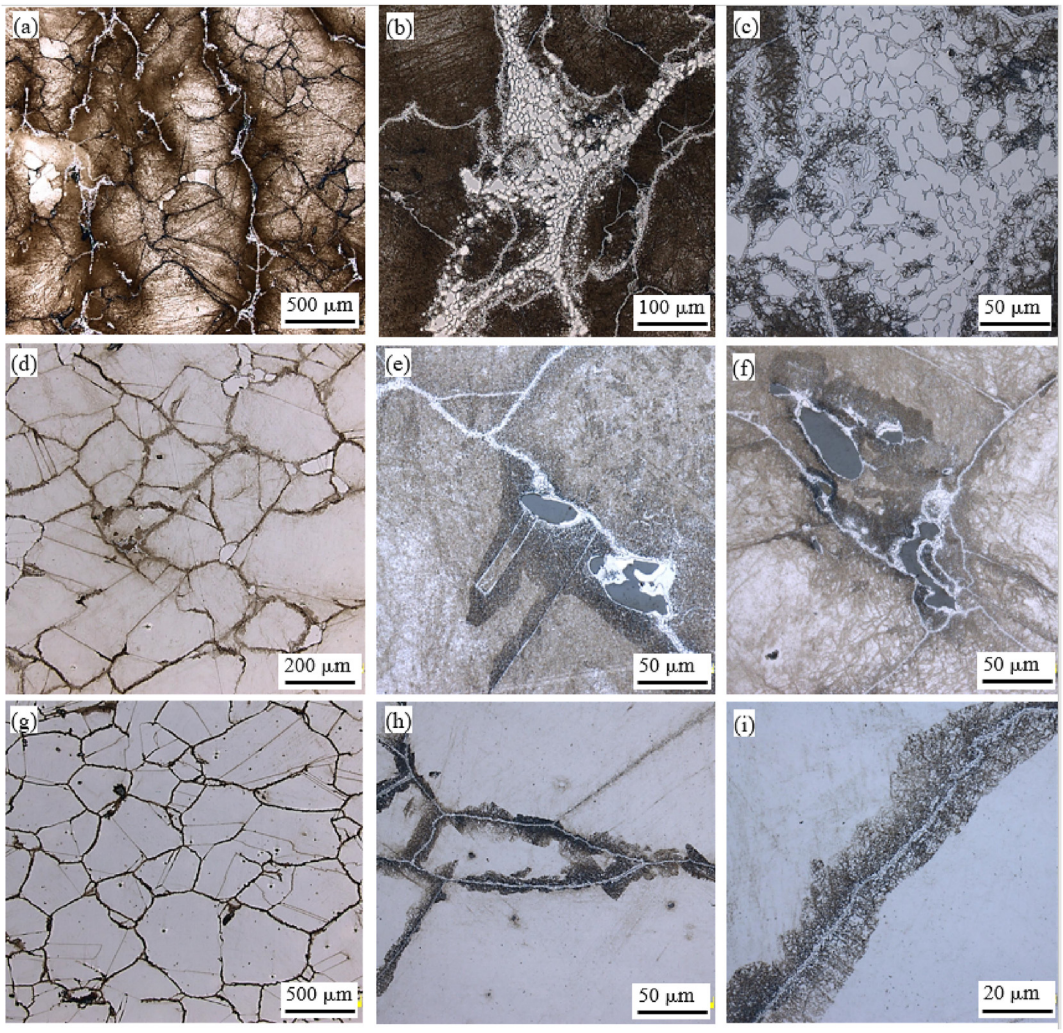


**Fig. 2 – Microstructure of deformed X38CrMo16 at 1204 °C etched by Villela (a–c): Center (d–f): Quarter (g–i): Surface.**

## 3. Results

### 3.1. *Microstructure analysis*

Optical microscopy observation of the ingot forged at 1204 °C, Fig. 2, revealed the presence of a white phase, primarily precipitated along the grain boundaries. The volume fraction of the white phase was different from the surface to the center regions. The highest amount was found in the center region and a notable decrease towards the surface. As shown in Fig. 2 (a-c), in the center region, the blocky and coarse white phase can be seen clearly, while in the quarter region, Fig. 2 (d-f), a few blocky precipitates as well as film-like phase along the grain boundary are present. As the distance from the center increases, the quantity of the white phase decreased in favor of a thin film-like along the grain boundary, Fig. 2 (g-i). The thickness of the film-like phase varied along the grain boundaries and was between 0.5 and 1 μm.

Fig. 3 shows illustrative examples of the microstructure of the three regions for the ingot which was forged at 1260 °C. Microscopic observation revealed the presence of coarse white phases, which were discontinuous and distributed locally, as opposed to what was observed when the forging was carried out at 1204 °C (Fig. 2).

Elemental analysis by EDS was conducted for ingots forged at 1204 °C and 1260 °C and the results are reported in Figs. 4 and 5, respectively. The analyses revealed that in both cases, a significant enrichment of alloying elements such as Cr, Mo, and C in the white phase as compared to the original composition of the steel (0.37% C, 15.21% Cr, and 1.1% Mo (wt.%)). The carbon contents reported in Figs. 4 and 5 could be compared with the nominal composition (0.37% C). However, it must be noted that although the EDS analyses were done using a high-resolution EDS detector (QUANTAX FlatQUAD) the obtained values are not absolute and should be regarded as relative only for comparison purposes.

In order to better identify the formation and composition of the white zones, simulation of phases formed between 500 °C and 1500 °C was carried out using Thermo-Calc software, and the results are reported in Fig. 6. It can be seen that during equilibrium solidification, the start temperature for $M_{23}C_6$ carbides precipitation is around 1100 °C and the stable phases at room temperature are ferrite, $M_{23}C_6$, $M_2P$, and MnS. As well,

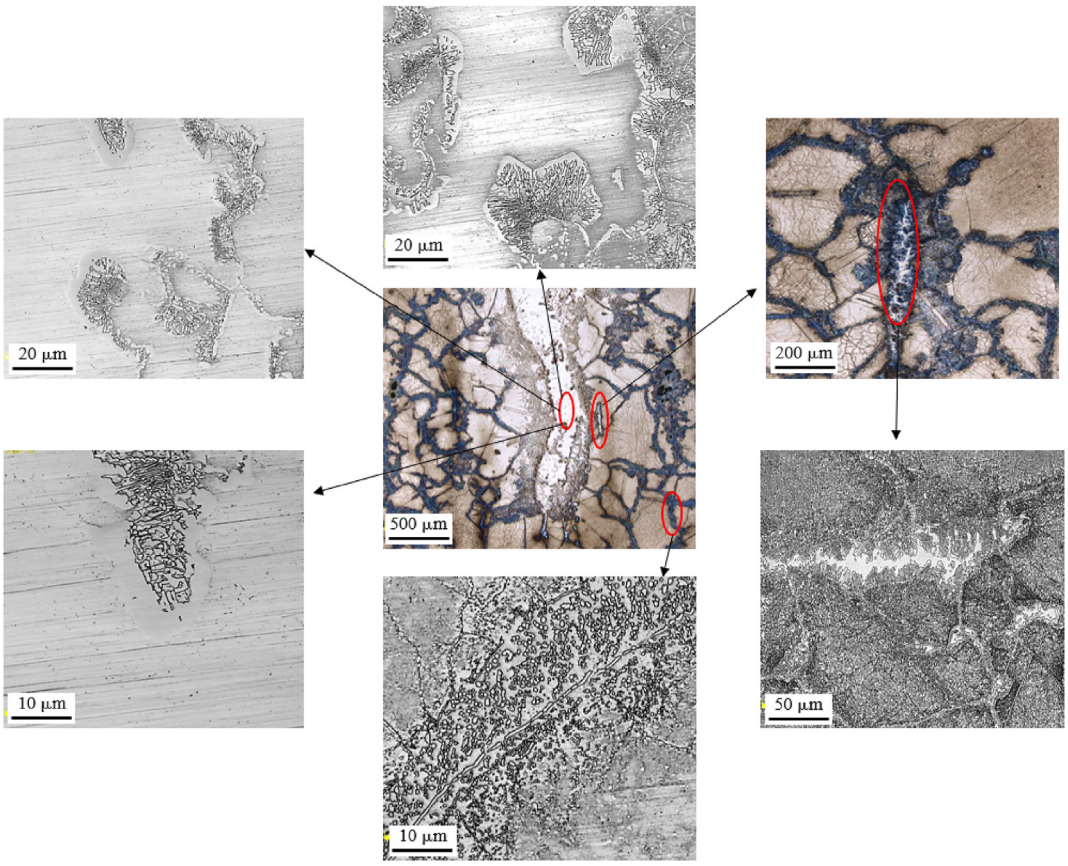


**Fig. 3 – Microstructure of deformed X38CrMo16 at 1260 °C etched by Villela.**

the eutectic temperature is 1243.42 °C with 20.5 %Cr and the primary ferrite structure starts to be formed when the temperature decreases to 1468.39 °C. The diagram would be more discussed in the next section.

X-ray diffraction data of the center of both ingots forged at 1260 °C and 1204 °C, extracted from a computer-controlled system, is presented in Fig. 7. The data were plotted in the form of the square root of x-ray intensity [Sqrt (counts/sec)]

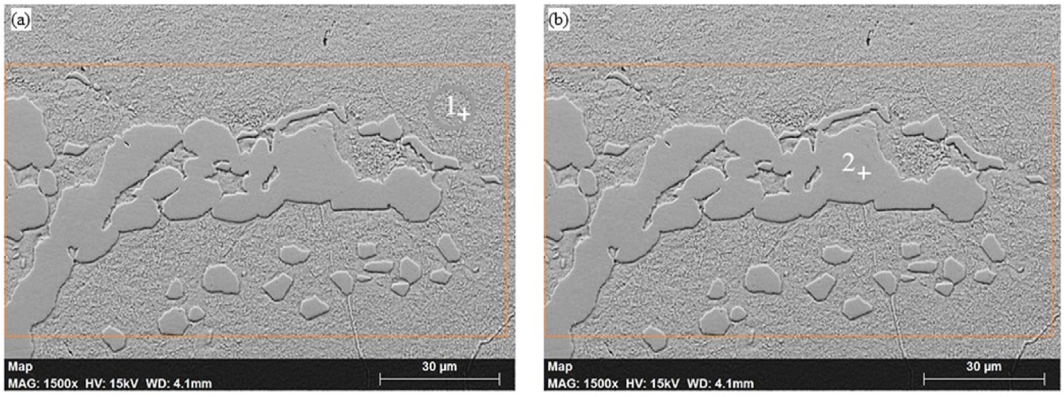


| Spectrum point (wt.%) | Fe | C | P | Cr | Ni | Mo | Mn |
|---|---|---|---|---|---|---|---|
| 1 | 78.71 | 2.41 | 0.07 | 16.46 | 0.23 | 1.54 | 0.58 |
| 2 | 32.05 | 4.05 | 0.32 | 58.48 | 0 | 2.09 | 0.41 |

**Fig. 4 – Chemical composition analysis measured by EDS for the ingot with 1204 °C forging temperature (a), Matrix. (b), White phase.**


| Spectrum | C | Al | Si | P | S | V | Cr | Fe | Cu | Nb | Mo | Mn |
|---|---|---|---|---|---|---|---|---|---|---|---|---|
| 1 | 2.41 | 0.11 | 0.21 | 0.06 | 0 | 0.37 | 61.97 | 28.2 | 0 | 0.15 | 6.20 | 0.51 |
| 2 | 1.84 | 0.04 | 0.59 | 0.07 | 0 | 0.07 | 14.48 | 80.59 | 0 | 0.01 | 1.24 | 1.07 |
| 3 | 1.82 | 0.03 | 0.51 | 0.03 | 0 | 0.02 | 13.04 | 82.72 | 0 | 0.01 | 0.73 | 0.89 |

**Fig.5 – Chemical composition analysis measured by EDS for the ingot with 1260 °C forging temperature.**

versus 2θ (degrees) to better reveal the weaker peaks. The 2θ range for the specimens of this study was between 20 and 90° with a step size of 0.02°. In Fig. 7, the peaks were indexed using highScore Plus software with standard database (PLU2020).

SEM micrograph and elemental map of the white phase by EDS is reported in Fig. 8 for both testing conditions. The figure depicts the significant reduction of Fe and a sharp increase in Cr and Mo. This observation confirms that the alloying element enrichment detected in the white phase is present along the interface between the matrix and the white phase.

## 4. Discussion

In ingot casting, the macrostructure of the as-cast material along the radial direction is composed of three distinct zones

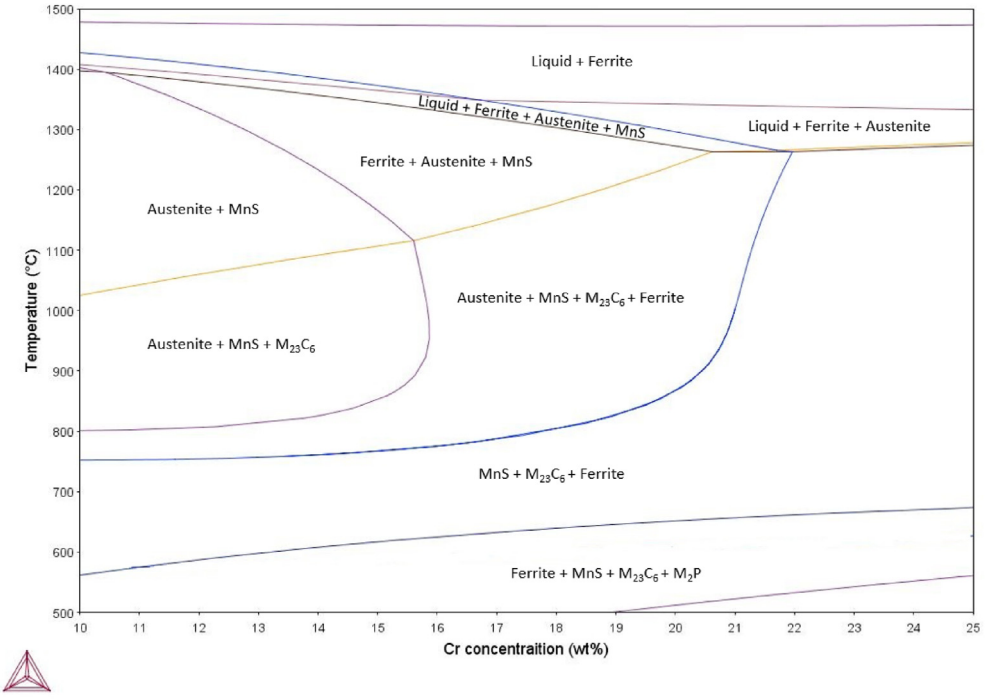


**Fig. 6 – Thermo-Calc phase diagram simulation between 500 °C and 1500 °C using the composition of Table 1.**

from the mold wall to the center of the ingot [24]. The significant magnitude of the temperature difference between the mold wall and the melt leads to the rapid cooling of the zones in contact with the wall resulting in the nucleation of equiaxed and fine grains forming what is commonly called the "chilled zone". With the advancement of the solidification interface, the temperature gradient decreases, and the crystals gradually grow dendritically in certain crystallographic directions. In this zone, the grains grow along a preferred orientation parallel to the heat flow direction, resulting in the formation of columnar grains. The third zone at the center of the ingot is called "equiaxed zone" which consists of equiaxed grains oriented randomly [25]. The above distinction of the three zones in the cast ingot will be used in the following to analyze the obtained results.

### 4.1. *Off- eutectic non-equilibrium solidification*

The non-equilibrium solidification process of large castings with off-eutectic composition may lead to two types of segregation [26]. There is macrosegregation which causes compositional variations over large distances (tens of centimeters), and there is microsegregation that takes place on the scale of grain boundaries and secondary dendrite arm spacing [2]. The extent of microsegregation depends on solidification conditions such as local cooling rates, thermal gradients, and changes in chemical composition. These factors control the migration of solutes at the solid/liquid interface so that by increasing the distance from the mold wall, the thermal gradient ahead of the solidification interface is gradually decreased and more solutes are released into the liquid. With the advancement of solidification, the residual melt, rich in solutes, primarily congregates in the root zones of the dendrites due to lower thermal dissipation in these zones. Consequently, the eutectic transformation takes place at the final solidification zones, dendrites, and grain boundaries and produces two composite solid phases (Ferrite + $M_{23}C_6$)$_e$.

As shown in Fig. 6, the equilibrium phase diagram predicted by Thermo-Calc, the phase sequence during the solidification process of X38CrMo16 includes:

$$L \rightarrow L + \text{Ferrite} \rightarrow L + \gamma + \text{Ferrite} \rightarrow L + \gamma + \text{Ferrite} + MnS \rightarrow \gamma + \text{Ferrite} + MnS \rightarrow \gamma + MnS \rightarrow \gamma + M_{23}C_6 + MnS \rightarrow \gamma + \text{Ferrite} + M_{23}C_6 + MnS \rightarrow \text{Ferrite} + M_{23}C_6 + MnS \rightarrow \text{Ferrite} + M_{23}C_6 + MnS + M_2P$$

And the eutectic transformation that occurs along the grain boundaries is:

$$L \rightarrow \text{Ferrite} + M_{23}C_6$$

It is shown in Fig. 6 that X38CrMo16 is an off-Eutectic alloy with 15.20 %Cr in nominal composit14ion and 21.5 %Cr in eutectic composition. By solidification proceeding, the solute distribution depends on the advancing rate of the solidification interface and the diffusion coefficient of the solute in the liquid phase. According to the Scheil equation [27], the solute distribution in a definite volume can be described by the following equation:

$$\underline{C_L} = C_0 f_L^{(K_E - 1)}$$

where $\underline{C_L}\left(\frac{mol}{L}\right)$ is the solute concentration in the residual melt, $C_0\left(\frac{mol}{L}\right)$ represents the initial solute concentration, $f_L$ is

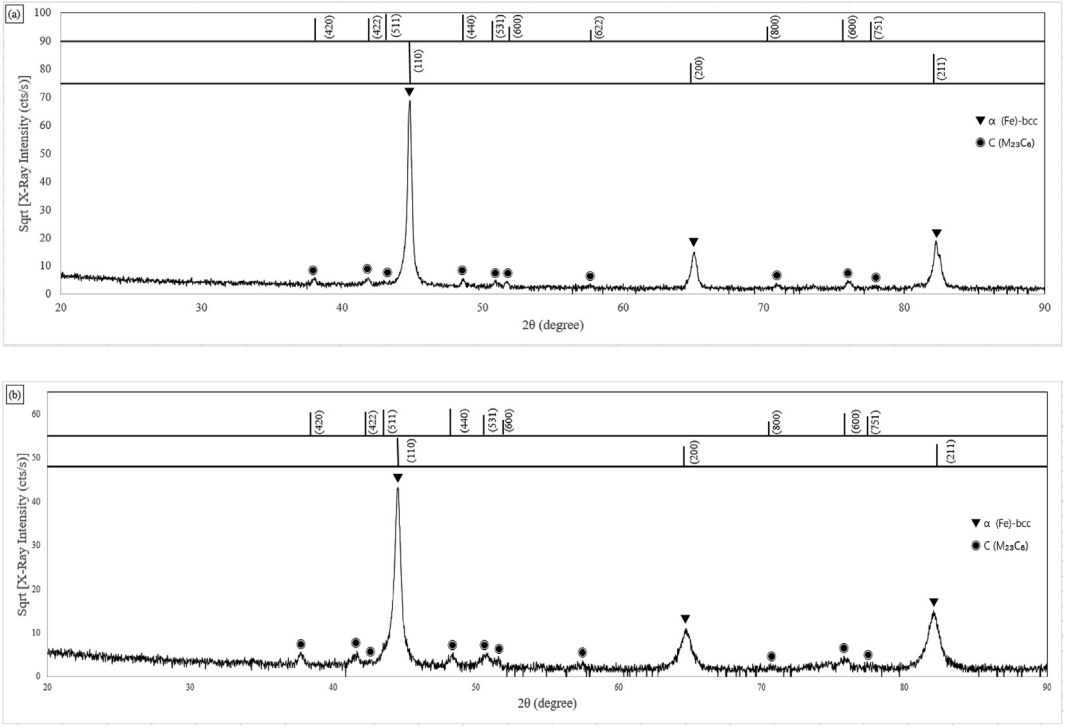


**Fig. 7 – XRD pattern of as polished X38CrMo16 specimen forged at (a), 1260 °C (b), 1204 °C.**

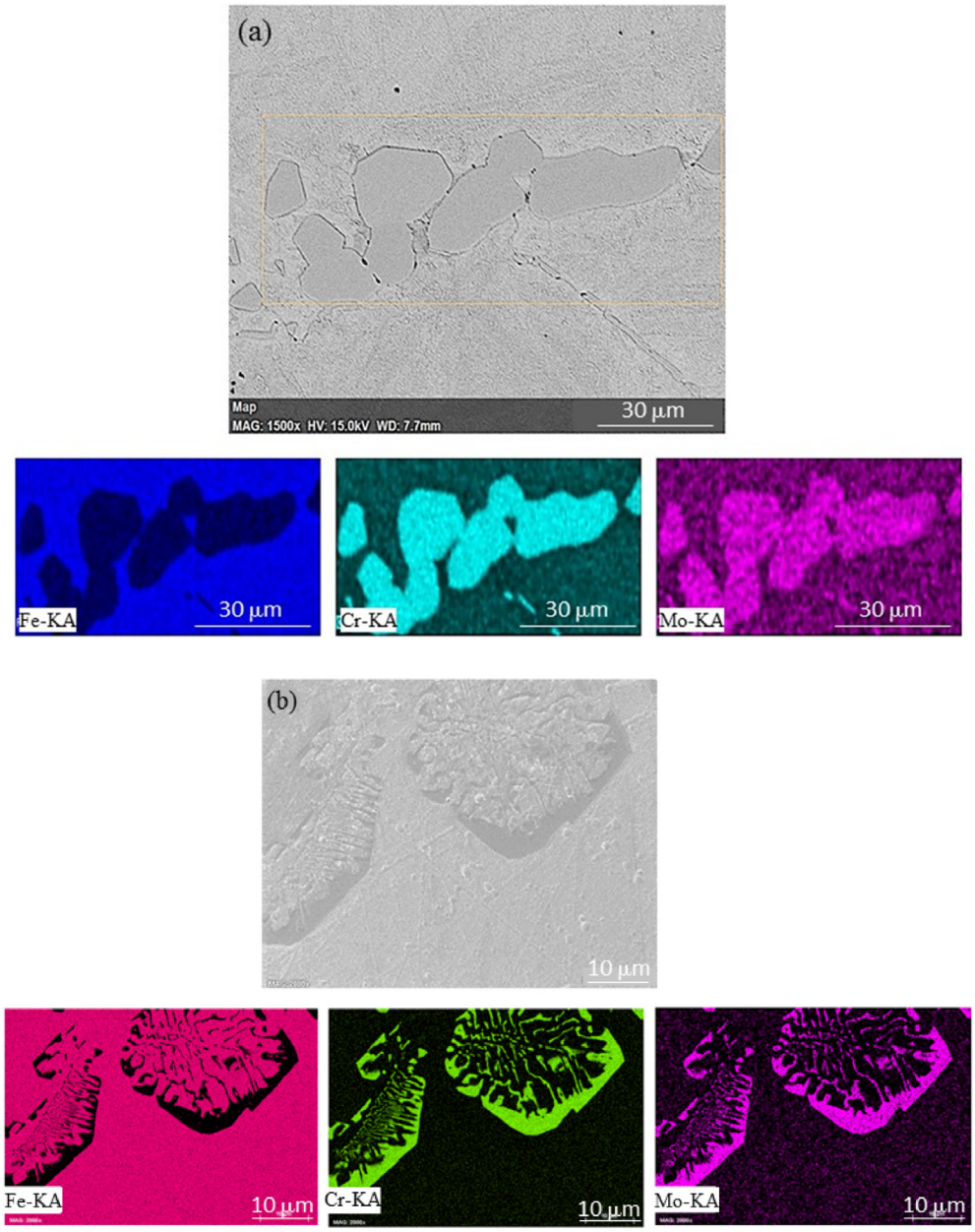


**Fig. 8 – SEM micrograph and elemental map by EDS of the white phase of forging temperature (a), 1204 °C (b), 1260 °C.**

the fraction of residual melt, and $K_E$ (the ratio of the concentration of a substance in one medium or phase to the concentration in a second phase) describes the effective partition coefficient. On the other hand, $K_E$ and solidification rate could be related to each other using the following relation reported by Burton et al. [28]:

$$K_E = \frac{K_0}{K_0 + (1 - K_0)exp\left(-\frac{R\delta_N}{D_L}\right)}$$

where $k_0$ is the equilibrium partition coefficient of solute, R $\left(\frac{m}{s}\right)$ is the solidification rate; $\delta_N$ $(m)$ the thickness of diffusion boundary layer in advance of the solidification interface; $D_L$ $\left(\frac{m^2}{s}\right)$ the diffusion coefficient of solute in a liquid phase. It is clear that the higher the $K_E$, the lower the $\underline{C_L}$ or the smaller the solute concentration in the residual melt.

In the chill zone, the cooling rate (R) is the highest, and a large number of grains nucleate simultaneously. The higher R leads to smaller $\underline{C_L}$ because of increasing $K_E$. Therefore, the solute partition during solidification is nearly suppressed. Under these conditions, most of the solutes are trapped in the pre-solidified grains and lower number of solute atoms are rejected into the melt in front of the solidification front. It can be seen in Fig. 2 (g-i) that the thin film-like eutectic carbides are precipitated along the grain boundaries. By taking distance from the mold wall (in the columnar zone), the thermal and constitutional supercooling as well as R becomes smaller and $\underline{C_L}$ increase correspondingly. So, more solutes are rejected into the bulk melt from the solidification

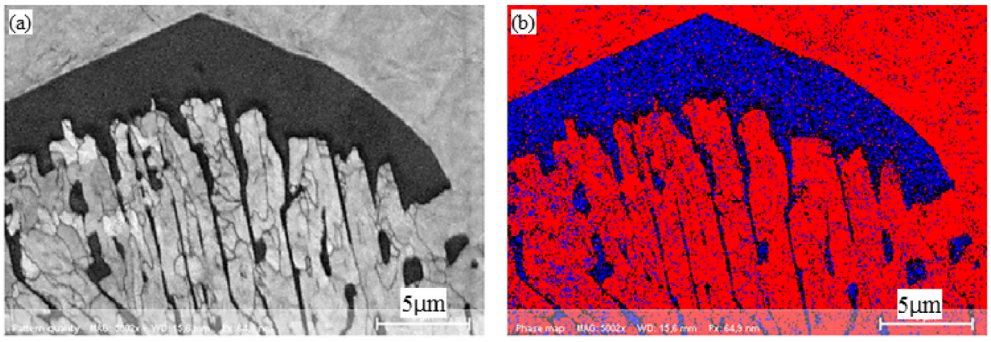


**Fig. 9 – EBSD orientation mapping of the specimen: (a), band-contrast image; (b), phase map (blue-$M_{23}C_6$ phase, red-ferrite phase).**

front. As shown in Fig. 2 (d-f), the liquid metal in the dendrite and grain boundary zones reaches the eutectic composition. At the center of the ingot (i.e. in the equiaxed zone), the thermal transfer is much smaller as compared with the two other zones and therefore after complete solidification, the eutectic carbides precipitate in the center of the ingot along the dendrite and grain boundaries, as revealed in Fig. 2 (a-c).

### 4.2. *Identification of the eutectic phase*

To detect and identify the eutectic phase, EBSD measurements were conducted by considered phases including Austenite-fcc, Ferrite-bcc, and chromium carbide. To identify the type of Carbide and other phases, we selected different types of chromium carbides and $M_{23}C_6$ was the best well-matched carbide with minimum zero solution percentage.

The results show that the chromium-rich regions could be related to $M_{23}C_6$ carbide (in blue) precipitated in a matrix of delta ferrite (in red), Fig. 9.

The distribution and volume fraction of the eutectic phase plays a crucial role in changing the mechanical properties, which may lead to cracking and part rejection during the forging operation. Therefore, the forging temperature must be adjusted in a way to do not reach the eutectic phase composition. Specifically, in the present study, the formation temperature of the eutectic phase is 1243.42 °C and thus the forging temperature of 1260 °C is higher than the eutectic temperature transformation. This means that the eutectic phase precipitated along the grain boundaries would be liquid when forging was carried out at 1260 °C. In contrast, when forging at 1204 °C, no liquid phase is expected to be present.

Very little or no data is available in the literature on the forging of high strength steels in presence of a liquid phase and its impact on crack initiation. Higashi et al. studied the effect of liquid phase on tensile elongation of superplastic aluminum alloys and reported that macroscopic melting begins to occur when forging temperature is higher than the eutectic temperature. They also found that, as the presence of the eutectic phase was increasing at the grain boundaries, the shear stress could not be transferred across them resulting in crack initiation [29]. In another study, Vaandrager and Pharr reported that by applying the stress, the liquid phase quickly redistributed and squeezes out of highly stressed boundaries and flows into less highly stressed boundaries. If the volume fraction of the liquid is increased, deformation proceeds by grain boundary sliding accommodated by the formation of cavities in the liquid which adversely affects the formability of the material [30]. Finally, in a recent publication, Yongnan et al. [31] investigated the effect of temperature on the segregation and deformation mechanism of $\alpha$+$Ti_2Cu$ alloy during semi-solid forging. They found that by increasing the forging temperature, a continuous liquid layer is formed at the grain boundaries that moves along the grain boundary during deformation and a significant amount, similar to a macrosegregated zone, of the $Ti_2Cu$ phase is formed.

In the present study, as reported in Fig. 3, at the higher forging temperature, the higher amount of the eutectic phase present in the material, results in the formation of continuous bands of large macrosegregated zones which could be the source of cracking; while at the lower forging temperature, a more discontinuous phase distribution is observed thereby reducing any cracking risk.

## 5. Conclusion

This research investigated the characteristics of eutectic phase precipitation as a function of the forging temperature in a large diameter ingot made of X38CrMo16 martensitic stainless steel and the following conclusion were obtained:

1. The eutectic carbides in the off-eutectic X38CrMo16 martensitic stainless steels primarily precipitated at the grain boundaries.
2. The morphology and distribution of the eutectic phase varied from the outer wall to the inner wall along the radial direction of the mold. Different morphologies consist of thin film-like carbides, skeleton-like and blocky carbides were revealed.

3. The volume fraction of the precipitated eutectic phase was affected by the cooling rate during solidification. Increasing the cooling rate suppressed the solute migration to the liquid phase which led to decreasing the amount of eutectic carbide. In contrast, a significant amount of eutectic phase precipitated along the grain boundaries at the center of the ingot which experiences the lowest cooling rate.
4. The type and composition of eutectic phases were determined through EBSD. The results indicated that alloying elements such as Cr, Mo, and C were aggregated remarkably on the eutectic carbide and the eutectic phase is a mixture of $M_{23}C_6$ + delta ferrite.
5. The equilibrium phase diagram of X38CrMo16 was simulated by Thermo-Calc software that was consistent with experimental results.

## Declaration of Competing Interest

The authors declare that they have no known competing financial interests or personal relationships that could have appeared to influence the work reported in this paper.

## Acknowledgments

The current research was conducted in close collaboration with Finkl Steel-Sorel as an industrial partner. The authors are grateful to Finkl Steel–Sorel for providing the specimens, as well as the full support of the R&D and engineering department. MITACS was supporting a portion of this research collaboration through a grant (IT164670) that is appreciatively acknowledged. We would also like to thank Dr. Mohammad Saadati for carrying out the EBSD characterization and his valuable input to analysis of EBSD images and Mr. Mazen Samara for conducting the XRD tests.

## REFERENCES

[1] Momeni A, Dehghani K, Heidari M, Vaseghi M. Modeling the flow curve of AISI 410 martensitic stainless steel. J Mater Eng Perform 2012;21:2238–43. https://doi.org/10.1007/s11665-012-0172-9.
[2] Loucif A, Fredj EB, Harris N, Shahriari D, Jahazi M, Lapierre-Boire L-P. Evolution of A-type macrosegregation in large size steel ingot after multistep forging and heat treatment. Metall Mater Trans B 2018;49:1046–55. https://doi.org/10.1007/s11663-018-1255-2.
[3] Suwas S, Ray RK. Texture evolution during solidification and solid-state transformation. Crystallographic texture of materials. Springer; 2014. p. 73–93. https://doi.org/10.1007/978-1-4471-6314-5.
[4] Miettinen J. Calculation of solidification-related thermophysical properties for steels. Metall Mater Trans B 1997;28:281–97. https://doi.org/10.1007/s11663-997-0095-2.
[5] Loucif A, Shahriari D, Zhang C, Jahazi M, Lapierre-Boire LP, Tremblay R. Macrosegregation of alloying elements in hot top of large size high strength steel ingot. Materials science forum. Trans Tech Publ; 2017. p. 1176–81. https://doi.org/10.4028/www.scientific.net/MSF.879.1176.
[6] Chadha K, Shahriari D, Jahazi M. Constitutive modelling of ingot breakdown process of low alloy steels. Metall. Ital 2016;4:5–12. https://doi.org/10.1007/978-981-10-4819-7_20.
[7] Dieter GE, Kuhn HA, Semiatin SL. Handbook of workability and process design. ASM International 2003. https://doi.org/10.1361/hwpd2003p003.
[8] Chadha K, Shahriari D, Tremblay R, Bhattacharjee PP, Jahazi M. Deformation and recrystallization behavior of the cast structure in large size, high strength steel ingots: experimentation and modeling. Metall Mater Trans 2017;48:4297–313. https://doi.org/10.1007/s11661-017-4177-8.
[9] Ghadar S, Momeni A, Tolaminejad B, Soltanalinezhad M. A comparative study on the hot deformation behavior of 410 stainless and K100 tool steels. Mater Sci Eng, A 2019;760:394–406. https://doi.org/10.1016/j.msea.2019.06.016.
[10] Kwon D, Asaro R. A study of void nucleation, growth, and coalescence in spheroidized 1518 steel. Metallurgical Transactions A 1990;21(1):117. https://doi.org/10.1007/BF02656430.
[11] Chae D, Koss D. Damage accumulation and failure of HSLA-100 steel. Mater Sci Eng, A 2004;366(2):299–309. https://doi.org/10.1016/j.msea.2003.08.040.
[12] Cowie JG, Tuler FR. The influence of second-phase dispersions on shear instability and fracture toughness of ultrahigh strength AISI 4340 steel. Mater Sci Eng, A 1991;141(1):23–37. https://doi.org/10.1016/0921-5093(91)90704-Q.
[13] Cox T, Low JR. An investigation of the plastic fracture of AISI 4340 and 18 Nickel-200 grade maraging steels. Metallurgical Transactions 1974;5(6):1457–70. https://doi.org/10.1007/bf02646633.
[14] Bettanini AM, Hannard F, Mithieux J-D, Badinier G, Jacques PJ, Pardoen T, et al. Residual ferrite in martensitic stainless steels: the effect of mechanical strength contrast on ductility. Mater Sci Eng, A 2018;731:495–505. https://doi.org/10.1016/j.msea.2018.06.012.
[15] Qi R-S, Jin M, Guo B-F, Liu X-G, Chen L. Hot-deformation behavior and hot-processing maps of AISI 410 martensitic stainless steel. High Temp Mater Process 2016;35:929–40. https://doi.org/10.1515/htmp-2015-0145.
[16] Matsubara Y, Sasaguri N, Shimizu K. Solidification and abrasion wear of white cast irons alloyed with 20% carbide forming elements. Wear 2001;250:502–10. https://doi.org/10.1016/S0043-1645(01)00599-3.
[17] Boccalini M, Goldenstein H. Solidification of high speed steels. Int Mater Rev 2001;46:92–115. https://doi.org/10.1179/095066001101528411.
[18] Guo J, Liu L, Li Q, Sun Y, Gao Y, Ren X, et al. Characterization on carbide of a novel steel for cold work roll during solidification process. Mater Char 2013;79:100–9. https://doi.org/10.1016/j.matchar.2013.02.011.
[19] Zhou X, Fang F, Li G, Jiang J. Morphology and properties of M2C eutectic carbides in AISI M2 steel. ISIJ Int 2010;50:1151–7. https://doi.org/10.2355/isijinternational.50.1151.
[20] Janovec J, Svoboda M, Blach J. Evolution of secondary phases 12% Cr steel during quenching and tempering. Mater Sci Eng, A 1998;249:184–9. https://doi.org/10.1016/S0921-5093(98)00526-7.
[21] Formenti A, Eliasson A, Mitchell A, Fredriksson H. Solidification sequence and carbide precipitation in Ni-base superalloys In718, In625 and In939. High Temp Mater Process 2005;24:239–58. https://doi.org/10.1515/HTMP.2005.24.4.239.
[22] Ebrahimi G, Keshmiri H, Momeni A. Effect of heat treatment variables on microstructure and mechanical properties of 15Cr–4Ni–0· 08C martensitic stainless steel. Ironmak Steelmak 2011;38:123–8. https://doi.org/10.1179/030192310X12816231892468.

[23] Kipelova A, Belyakov A, Kaibyshev R. The crystallography of M23C6 carbides in a martensitic 9% Cr steel after tempering, aging and creep. Phil Mag 2013;93:2259–68. https://doi.org/10.1080/14786435.2013.765995.
[24] Pineda D, Martorano M. Columnar to equiaxed transition in directional solidification of inoculated melts. Acta Mater 2013;61:1785–97. https://doi.org/10.1016/j.actamat.2012.12.002.
[25] Uddagiri M, Spee J, Hubig S, Steinbach I. Columnar-equiaxed transition in continuous casting based on a micro-macro solidification model with long-range solutal mixing. IOP conference series: materials science and engineering. IOP Publishing; 2020, 012014. https://doi.org/10.1088/1757-899X/861/1/012014.
[26] Porter DA, Easterling KE. Phase transformations in metals and alloys (revised reprint). CRC press; 2009. https://doi.org/10.1201/9781439883570-10.
[27] Wu X, Jing H, Zheng Y, Yao Z, Ke W, Hu Z. The eutectic carbides and creep rupture strength of 25Cr20Ni heat-resistant steel tubes centrifugally cast with different solidification conditions. Mater Sci Eng, A 2000;293:252–60. https://doi.org/10.1016/S0921-5093(00)00984-9.
[28] Burton J, Prim R, Slichter W. The distribution of solute in crystals grown from the melt. Part I. Theoretical. J Chem Phys 1953;21:1987–91. https://doi.org/10.1063/1.1698728.
[29] Higashi K, Nieh T, Mabuchi M, Wadsworth J. Effect of liquid phases on the tensile elongation of superplastic aluminum alloys and composites. Scripta Metall Mater 1995;32:1079–84. https://doi.org/10.1016/0956-716x(94)00003-z.
[30] Vaandrager B, Pharr G. Compressive creep of copper containing a liquid bismuth intergranular phase. Acta Metall 1989;37:1057–66. https://doi.org/10.1016/0001-6160(89)90102-8.
[31] Yongnan C, Chuang L, Fengying Z, Jianfeng W, Yongqing Z. Effect of temperature on segregation and deformation mechanism of α+ Ti2Cu alloy during semi-solid forging. Rare Met Mater Eng 2015;44:1369–73. https://doi.org/10.1016/S1875-5372(15)30091-6.